Granular Matter (2012) 14:115–120
DOI 10.1007/s10035-012-0324-5

ORIGINAL PAPER

Oblique impact of frictionless spheres: on the limitations of hard sphere models for granular dynamics

Patric Müller · Thorsten Pöschel

Received: 10 August 2011 / Published online: 22 February 2012

Abstract When granular systems are modeled by hard spheres, particle–particle collisions are considered as instantaneous events. This implies that while the velocities change according to the collision rule, the positions of the particles are the same before and after such an event. We show that depending on the material and system parameters, this assumption may fail. For the case of viscoelastic particles we present a universal condition which allows to assess whether hard-sphere modeling and, thus, event-driven Molecular Dynamics simulations are justified.

Keywords Granular gases · Hard sphere model · Coefficient of normal restitution · Viscoelastic spheres · Event-driven molecular dynamics

1 Introduction

Hard sphere modelling of granular systems assumes that the dynamics of the system may be described as a sequence of *instantaneous* events of *binary* collisions. In between the collisions the particles move freely along straight lines, or ballistic trajectories in presence of external fields like gravity. The hard-sphere model of particle collisions is the foundation of both Kinetic Theory of granular matter, based on the Boltzmann equation, e.g. [1–3], and event-driven Molecular Dynamics (eMD) of granular matter, e.g. [4–6].

In hard sphere approximation, the inelastic collision of frictionless spheres i and j located at $\mathbf{r}_i$ and $\mathbf{r}_j$ traveling at velocities $\dot{\mathbf{r}}_i$ and $\dot{\mathbf{r}}_j$ is, thus, characterized by the collision rule describing the instantaneous exchange of momentum between the colliders,

$$\left(\dot{\mathbf{r}}_i' - \dot{\mathbf{r}}_j'\right) \cdot \hat{e}_r' = -\varepsilon \left(\dot{\mathbf{r}}_i^0 - \dot{\mathbf{r}}_j^0\right) \cdot \hat{e}_r^0 \tag{1}$$

with the unit vector $\hat{e}_r \equiv \left(\mathbf{r}_i - \mathbf{r}_j\right) / \left|\mathbf{r}_i - \mathbf{r}_j\right|$. Upper index 0 describes values just before the collision, primed values describe postcollisional values. Inelasticity is characterized by the coefficient of (normal) restitution ε.

The instantaneous character of the collisions implies that as the result of a collision only the velocities of the particles change but not their positions, $\mathbf{r}_i' = \mathbf{r}_i^0$, $\mathbf{r}_j' = \mathbf{r}_j^0$ and, thus, $\hat{e}_r' \equiv \hat{e}_r^0$. With this, Eq. (1) turns into

$$\left(\dot{\mathbf{r}}_i' - \dot{\mathbf{r}}_j'\right) \cdot \hat{e}_r^0 = -\varepsilon^{\mathrm{HS}} \left(\dot{\mathbf{r}}_i^0 - \dot{\mathbf{r}}_j^0\right) \cdot \hat{e}_r^0 \tag{2}$$

which allows to compute the postcollisional velocities successively for all collisions in the system, which is the basic idea of eMD. Provided the system may be described as hard spheres undergoing instantaneous collisions, eMD may be by orders of magnitude more efficient than ordinary MD integrating Newton's equation of motion. Recently, extremely efficient algorithms for eMD simulations have been developed, e.g. [7].

As physical particles are not perfectly hard but the collision is governed by *finite* interaction forces, the hard sphere model is an idealization whose justification may be challenged. Especially in view of its importance for Kinetic Theory and numerical simulation techniques. In particular, for finite duration of the collisions the unit vector $\hat{e}_r$ may rotate during a collision by the angle

Electronic supplementary material The online version of this article (doi:10.1007/s10035-012-0324-5) contains supplementary material, which is available to authorized users.

We dedicate this paper to the memory of Prof. Isaac Goldhirsch who passed away when on Sabbatical leave at our institute.

P. Müller (✉) · T. Pöschel
Institute for Multiscale Simulation, Universität Erlangen-Nürnberg, Erlangen, Germany
e-mail: patric.mueller@cbi.uni-erlangen.de

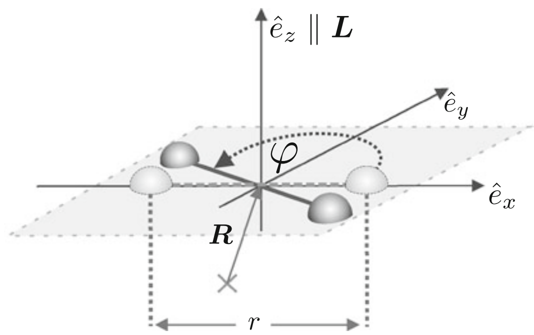

Fig. 1 Illustration of the used polar coordinates (see text)

$$\alpha \equiv \arccos\left(\hat{e}_r^0 \cdot \hat{e}_r'\right) \tag{3}$$

invalidating Eq. (2) and, therefore, the hard-sphere approximation. While this angle is negligible for approximately central impacts of relatively stiff spheres, it is not for oblique impacts of soft spheres [8].

Within this work we quantify under which conditions and to what extent the condition, $\hat{e}_r' \approx \hat{e}_r^0$, of the hard sphere assumption fails. The aim of the present paper is to provide a universal condition which allows, for *arbitrary* collisions of *arbitrary* elastic spheres, to assess whether the hard sphere model is acceptable for the description of particle collisions. Thus, we discriminate whether the hard sphere model is acceptable for systems, characterized by (i) a set of material parameters, (ii) particle sizes and (iii) a typical (thermal) impact velocity. To generalize our result to the case of inelastic collisions, we show that regarding the rotation angle α, elastic spheres are the marginal case, that is, if $\hat{e}_r' \approx \hat{e}_r^0$ holds true for elastic particles, it *certainly* holds true for inelastic particles.

2 Collision of spheres

Consider colliding spheres of masses m_i and m_j located at $\mathbf{r}_i$ and $\mathbf{r}_j$ and traveling with velocities $\dot{\mathbf{r}}_i$ and $\dot{\mathbf{r}}_j$. With the interaction force $\mathbf{F}$, their motion is described by

$$m_{\text{eff}}\ddot{\mathbf{r}} = \mathbf{F}\,, \qquad \ddot{\mathbf{R}} = \mathbf{0} \tag{4}$$

where

$$\mathbf{R} \equiv \frac{m_i\mathbf{r}_i + m_j\mathbf{r}_j}{m_i + m_j}\,, \quad \mathbf{r} = \mathbf{r}_i - \mathbf{r}_j\,, \quad m_{\text{eff}} = \frac{m_i m_j}{m_i + m_j} \tag{5}$$

are the center of mass coordinate, the relative coordinate and the effective mass, respectively. The center of mass moves due to external forces such as gravity and separates from the relative motion which in turn contains the entire collision dynamics.

For frictionless particles, the interaction force acts in the direction of the inter-center unit vector, $\mathbf{F} = F_n\hat{e}_r$, that is, there is no tangential force and, thus, the particles' rotation is not affected by the collision. During the collision the (orbital) angular momentum is conserved which allows for the definition of a constant unit vector $\hat{e}_L$:

$$\mathbf{L} = m_{\text{eff}}\,\mathbf{r} \times \dot{\mathbf{r}} \equiv L\hat{e}_L\,. \tag{6}$$

Thus, with the coordinate system spanned by

$$\hat{e}_x \equiv \hat{e}_r^0\,, \quad \hat{e}_z \equiv \hat{e}_L\,, \quad \hat{e}_y \equiv \hat{e}_z \times \hat{e}_x \tag{7}$$

and with its origin in the center of mass $\mathbf{R}$, the collision takes place in the $\hat{e}_x - \hat{e}_y$–plane.[1] In the collision plane we formulate the equation of motion in polar coordinates $\{r, \varphi\}$ (see Fig. 1):

$$m_{\text{eff}}r^2\dot{\varphi} = L\,, \quad m_{\text{eff}}\ddot{r} = F_c + F_n = m_{\text{eff}}r\dot{\varphi}^2 + F_n\,, \tag{8}$$

with the centrifugal force F_c. With the inital conditions

$$r(0) = r^0\,, \quad \dot{r}(0) = \dot{r}^0\,, \quad \varphi(0) = 0\,, \tag{9}$$

Eq. (8) fully describes the collision dynamics for an arbitrary normal force F_n. The collision terminates at time $t = \tau$ where [9,10]

$$\dot{r}(\tau) > 0 \quad \text{and} \quad F_n = 0. \tag{10}$$

Inserting the first equation of Eq. (8) into the second, we obtain

$$m_{\text{eff}}\ddot{r} = \frac{L^2}{m_{\text{eff}}r^3} + F_n \tag{11}$$

which fully governs the radial dynamics of the problem.

Note that in contrast to earlier work [9,10] where the coefficient of normal restitution was derived from force laws F_n here we allow the normal vector $\hat{e}_r$ to rotate during the collision and do not neglect the resulting centrifugal force.

Since for *any* finite interaction forces, the duration τ of a collision is finite, for non-central collisions, $\mathbf{L} \neq 0$, during the collision the spheres rotate around their center of mass, that is, $\hat{e}_r' \neq \hat{e}_r^0$ and $\alpha \neq 0$, see Eq. (3).

It is frequently stated that the hard sphere approximation and thus event-driven simulations are always justified for dilute systems where the mean free flight time of the particles is large compared to the typical collision time. Obviously, this condition is insufficient. It may be shown that the characteristics of dilute granular gases such as the coefficient of self diffusion sensitively depends on the rotation of the unit vector. [11].

[1] For central collisions we have $\mathbf{L} = \mathbf{0}$. In this case $\hat{e}_z$ may be any unit vector perpendicular to $\hat{e}_x$, $(\hat{e}_x \cdot \hat{e}_z = 0)$.

3 Elastic spheres

3.1 Dimensionless equation of motion

The collision of elastic spheres obeys Hertz' contact force [12],

$$F_n = F_n^{\text{el}} = \rho (l - r)^{3/2}\,, \qquad l \equiv r^0 = R_i + R_j\,, \tag{12}$$

where l denotes the distance between the particle centers at the moment of impact. The quantity $\xi \equiv l - r$ is often referred to as the deformation or mutual compression. The elastic constant ρ reads

$$\rho \equiv \frac{2Y\sqrt{R_{\text{eff}}}}{3(1-\nu^2)}\,, \tag{13}$$

where Y, ν and R_{eff} stand for the Young modulus, the Poisson ratio and the effective radius $R_{\text{eff}} = R_i R_j/(R_i + R_j)$, respectively.

Writing the general equation of motion Eq. (8) with the force given by Eq. (12) and measuring length in units of X and time in units of T [10],

$$X \equiv \frac{(-\dot{r}^0)^{4/5}}{k^{2/5}}\,, \quad T \equiv \frac{1}{k^{2/5}(-\dot{r}^0)^{1/5}}\,, \quad k \equiv \frac{\rho}{m_{\text{eff}}}\,, \tag{14}$$

we obtain

$$\frac{\mathrm{d}\varphi}{\mathrm{d}\tilde{t}} = \frac{c_\varphi}{\tilde{r}^2}\,, \qquad \frac{\mathrm{d}^2\tilde{r}}{\mathrm{d}\tilde{t}^2} = \tilde{r}\left(\frac{\mathrm{d}\varphi}{\mathrm{d}\tilde{t}}\right)^2 + \left(\tilde{l} - \tilde{r}\right)^{3/2} \tag{15}$$

with

$$\tilde{t} \equiv \frac{t}{T}, \quad \tilde{r} \equiv \frac{r}{X}, \quad \tilde{l} \equiv \frac{l}{X} \tag{16}$$

$$c_\varphi \equiv \frac{T}{X^2}\frac{L}{m_{\text{eff}}}. \tag{17}$$

The scaled initial conditions read

$$\varphi(0) = 0, \quad \tilde{r}(0) = \tilde{l} \quad \text{and} \quad \dot{\tilde{r}}(0) = 1. \tag{18}$$

According to Eq. (15) with the initial conditions Eq. (18), the binary collision of frictionless elastic spheres is described by only two free parameters: $\tilde{l}$ and c_φ.

3.2 Rotation of the normal vector

We solve the equations of motion (15) and (18) to obtain the rotation α of the unit vector, $\hat{e}_r$, given by Eq. (3) as a consequence of the collision of elastic spheres. This rotation occurs for oblique impacts and is commonly neglected in hard sphere simulations as well as in the Kinetic Theory of granular gases. Obviously, α depends on the material properties, particle sizes and on the geometry of the collision as sketched in Fig. 2.

To illustrate the fact that the rotation of the unit vector is by far not a small effect even for rather common systems, in Fig. 3 we plot the angle α as a function of the impact eccentricity d/l (see Fig. 2). The system parameters (in physical units) are: radii $R_1 = R_2 = 0.1\,\text{m}$, material density $\rho_m = 1,140\,\text{kg/m}^3$, Young modulus $Y = 10^7\,\text{N/m}^2$, Poisson ratio $\nu = 0.4$, impact velocity $20\,\text{m/s}$ (material parameters corresponding to hard rubber).

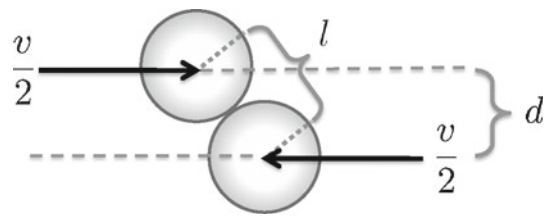

Fig. 2 Eccentric binary collision of spheres. The sketched situation corresponds to the eccentricity $d/l \approx 0.8$ where the rotation angle drawn in Fig. 3 adopts its maximum

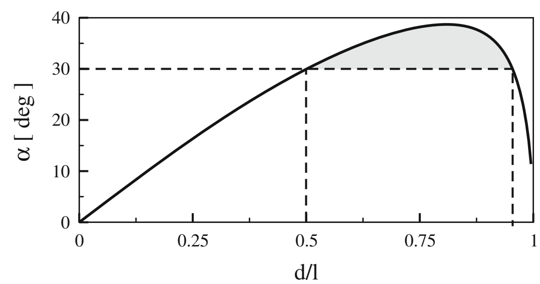

Fig. 3 Rotation angle α of the unit vector $\hat{e}_r$ as a function of the impact eccentricity d/l (see Fig. 2) for rubber spheres, parameters specified in the text. The marked area shows the interval where $\alpha > 30°$ corresponding to 65% of all collisions when molecular chaos is assumed

As expected, the rotation vanishes for central collisions. The rotation adopts its maximum for $d/l \approx 0.8$ (this situation corresponds to the sketch in Fig. 2) where it can easily reach values of $\alpha \approx 40°$. The position of the maximum may surprise since in the Kinetic Theory it is frequently assumed that if at all only rare *glancing collisions* might deserve a special consideration. Assuming molecular chaos, that is, $e \equiv d/l$ is distributed as $\mathrm{d}p(e) = 2e\,\mathrm{d}e$, and the parameters given above, about 65% of the collisions lead to a rotation angle $\alpha > 30°$ (marked interval in Fig. 3). Consequently, the rotation of the unit vector $\hat{e}_r$ is a significant effect for granular gases. Particularly for relatively soft materials (like e.g. hard rubber or nylon).

3.3 Universal description of the rotation angle

For elastic particles the dimensionless equation of motion of the collision (Eqs. 15 and 18) is fully specified by two independent parameters, $\tilde{l}$ and c_φ, defined in Eqs. (16) and (17). Therefore all material and system parameters may be mapped to a point in the $(\tilde{l}, c_\varphi)$-space. The rotation angle α can be determined by the following procedure:

Table 1 Parameter space scanned to obtain Fig. 4

	Unit	Min.	Max.	
Y	$(10^9\ \mathrm{N/m^2})$	0.01	100	Young's modulus
ν	–	0.2	0.5	Poisson ratio
R	(m)	0.001	0.1	Particle radius
ρ_m	$(\mathrm{kg/m^3})$	250	3,250	Material density
v	(m/s)	0.001	25	Impact velocity
d/l	–	0.01	0.99	Eccentricity

For the definition of impact velocity and eccentricity see Fig. 2

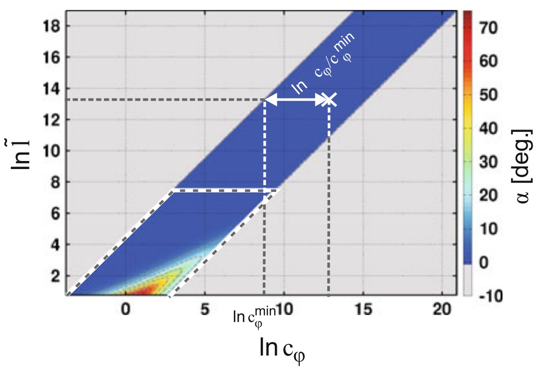

Fig. 4 Rotation angle α as function of $\tilde{l}$ and c_φ. Gray regions indicate points which do not correspond to any combination of parameters given in Table 1. (Color figure online)

1. Determine the dimensionless parameters: $\{Y, \nu, R, \rho_m, v, d/l\} \rightarrow \{\tilde{l}, c_\varphi\}$
2. Solve numerically the equations of motion, Eqs. (15, 18) for $0 \le t \le \tau$ where τ is the time when the collision terminates. τ is determined by the conditions $\ddot{\tilde{r}}(\tau) = 0$ and $\dot{\tilde{r}}(\tau) > 0$ (see Eq. 10).
3. The rotation angle is obtained from $\alpha = \varphi(\tau)$.

We performed this procedure for a wide range of relevant (physical) parameters given in Table 1. In dimensionless variables, this range corresponds to the interval

$$2.12 \le \tilde{l} \le 1.8 \cdot 10^9\,, \quad 2.12 \cdot 10^{-2} \le c_\varphi \le 1.26 \cdot 10^9\,. \tag{19}$$

Figure 4 shows the rotation angle α as a function of $\tilde{l}$ and c_φ on a double logarithmic scale.

From the definitions of $\tilde{l}$, c_φ, $\mathbf{L}$, Eqs. (6, 16, 17) and

$$\frac{X}{T} = -\dot{\mathbf{r}}^0 = v\sqrt{1-\left(\frac{d}{l}\right)^2} \tag{20}$$

which follows from the definitions, Eq. (14), and geometry (see Fig. 2), one obtains

$$\ln \tilde{l} = \ln\left(c_\varphi\right) + \frac{1}{2}\ln\left[\left(\frac{l}{d}\right)^2 - 1\right]. \tag{21}$$

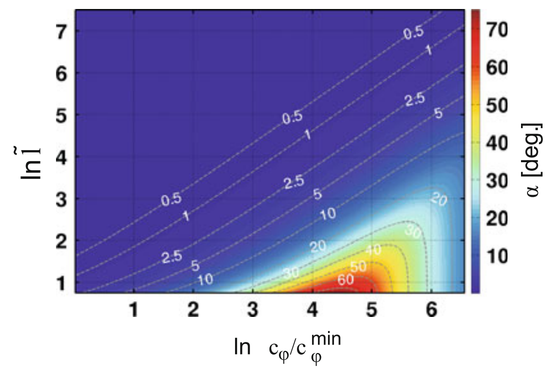

Fig. 5 Rotation angle α as function of $\tilde{l}$ and $c_\varphi/c_\varphi^{\min}$

This equation provides some insight into the structure of Fig. 4 and allows for a more intuitive presentation of the result. For fixed eccentricity d/l due to Eq. (21), in the double logarithmic scale used in Fig. 4, $\tilde{l}$ is a linear function of c_φ with slope 1. That is, all collisions taking place at the same impact eccentricity d/l are located on a straight line of slope 1 in the $(\ln c_\varphi, \ln \tilde{l})$-space. The position along this line is then determined by the remaining system parameters.

The chosen interval, $0.01 \le d/l \le 0.99$, see Table 1, implies that the intercept, of all possible straight lines given by Eq. (21) is bound to the range

$$-1.95 \le \ln \tilde{l}\Big|_{c_\varphi=0} \le 4.61\,, \tag{22}$$

which explains the stripe structure of the data in Fig. 4. All $(\ln \tilde{l}, \ln c_\varphi)$-pairs outside the colored stripe *cannot* be adopted for any combination of the parameters listed in Table 1 which is indicated by the gray areas in Fig. 4.

Figure 4 indicates that among all studied combinations of parameters only those for $-3 \lessapprox \ln c_\varphi \lessapprox 9$ and $1 \lessapprox \ln \tilde{l} \lessapprox 8$ (dashed region in Fig. 4) may lead to a noticeable rotation angle α or a significant deviation from the hard sphere model respectively. Therefore, we draw this region with a higher resolution of c_φ and $\tilde{l}$, see Fig. 5. In order to avoid the irrelevant gray regions, we plot the data over $\ln c_\varphi - \ln c_\varphi^{\min}$ instead of $\ln c_\varphi$ with

$$\ln c_\varphi^{\min} = \ln \tilde{l} - \frac{1}{2}\ln\left[\frac{1}{\left(\frac{d}{l}\right)^2_{\min}} - 1\right] \approx \ln \tilde{l} - 4.61 \tag{23}$$

as obtained from Eq. (21) with $(d/l)_{\min}$ taken from Table 1 (see illustration of $\ln c_\varphi - \ln c_\varphi^{\min}$ in Fig. 4).

The isolines of constant rotation angle α drawn in Fig. 5 indicate that there is a rather sharp transition between the regions where $\alpha \approx 0$ and $\alpha \gg 0$ in the $(\ln c_\varphi, \ln \tilde{l})$-space. Hence, regarding the rotation of the unit vector $\hat{e}_r$, the regions in the parameter space where the hard sphere model is a justifiable approximation are clearly separated from those where the hard sphere approximation is questionable.

3.4 Confidence regions of the hard sphere model

For practical applications one might wish to know whether a given set of material and system parameters allows for a hard-sphere description. One important prerequisite for the hard sphere model is a reasonable small rotation angle α (see Eq. 3). For the following we assume that the rotation angle α_c is marginally acceptable for the hard sphere approximation and provide a simple approximate method to decide whether the given system fulfills the above criterion of small rotation angles.

Figure 5 shows that for rotation angles up to about 15°, the isolines of constant rotation angle are approximately straight lines of slope $\overline{m} \approx 0.84$ on average. The corresponding intercept t_{α_c} decreases with the isoline value α_c. From Fig. 5 we obtain $t_{1^\circ} \approx 0.9$, $t_{5^\circ} \approx -0.29$, $t_{10^\circ} \approx -0.74$ and $t_{15^\circ} \approx -0.85$.

We specify a collision by

$$\ln \frac{c_\varphi}{c_\varphi^{\min}} = 4.61 - \frac{1}{2} \ln \left[\left(\frac{l}{d} \right)^2 - 1 \right],$$
$$\tilde{l} = \left[\frac{2Y\sqrt{R_{\text{eff}}}}{3(1-\upsilon^2)m_{\text{eff}}} \right]^{2/5} \left[\upsilon \sqrt{1-(d/l)^2} \right]^{-4/5} l \qquad (24)$$

and define

$$D_{\alpha_c} \equiv \ln \tilde{l} - \left(\overline{m} \ln \left(c_\varphi / c_\varphi^{\min}\right) + t_{\alpha_c} \right). \qquad (25)$$

$D_{\alpha_c} > 0$ indicates that the maximally expected rotation angle is smaller than α_c, that is, the hard sphere model is acceptable for this situation.

4 Inelastic spheres

4.1 Equation of motion

The main conclusion of this Section will be that inelastic interaction forces which are, perhaps, the most characteristic feature of granular materials, do not lead to an increase of the rotation angle α as compared with the elastic case detailed in the previous Section. Here, we exemplarily discuss a particular dissipation mechanism, the viscoelastic model which is widely used for modeling granular systems, e.g. [13–15]. Many other dissipative interaction forces as for instance plastic deformation or linear dashpot damping, lead to very similar results.

The collision of viscoelastic spheres is characterized by the interaction force [16]

$$F_n = F_n^{\text{el}} + F_n^{\text{dis}} = \rho(l-r)^{3/2} - \frac{3}{2} A\rho\dot{r}\sqrt{l-r} \qquad (26)$$

with the dissipative constant A being a function of the elastic and viscous material parameters [16] and the other parameters as described before. The collision terminates at time τ

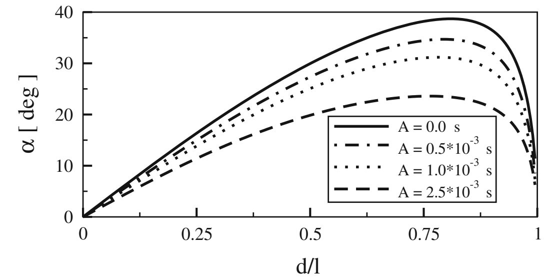

Fig. 6 Rotation angle α of the unit vector $\hat{e}_r$ as function of the eccentricity for various dissipative constants A. The elastic parameters are the same as for Fig. 3

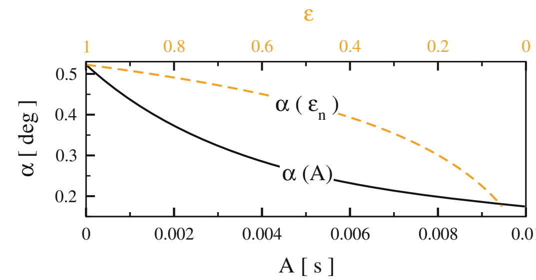

Fig. 7 Rotation angle α over the dissipative parameter A (lower scale, *full line*) and over the coefficient of normal restitution ε (upper scale, *dashed line*) for $d/l = 0.5$

when $\dot{r}(\tau) > 0$ and $\ddot{r}(\tau) = 0$, corresponding to purely repulsive interaction, see [10]. The dissipative part, F_n^{dis}, was first motivated in [17] and then rigorously derived in [16] and [18], where only the approach in [16] leads to an analytic expression of the material parameter A.

We apply the same scaling as in Sect. 3.1 to obtain

$$\frac{\mathrm{d}\varphi}{\mathrm{d}\tilde{t}} = \frac{c_\varphi}{\tilde{r}^2}$$
$$\frac{\mathrm{d}^2\tilde{r}}{\mathrm{d}\tilde{t}^2} = \tilde{r}\left(\frac{\mathrm{d}\varphi}{\mathrm{d}\tilde{t}}\right)^2 + \left(\tilde{l}-\tilde{r}\right)^{3/2} - c_{\text{dis}}\sqrt{\tilde{l}-\tilde{r}}\,\frac{\mathrm{d}\tilde{r}}{\mathrm{d}\tilde{t}} \qquad (27)$$

with the definitions and initial conditions given in Eqs. (16, 17, 18) and additionally

$$c_{\text{dis}} \equiv \gamma\sqrt{XT}\,; \qquad \gamma \equiv \frac{3}{2}\frac{\rho A}{m_{\text{eff}}}. \qquad (28)$$

In contrast to the case of elastic spheres discussed in Sect. 3, for inelastic frictionless spheres we need three independent parameters to describe their collisions, $\tilde{l}$, c_φ and c_{dis}.

4.2 The role of inelasticity

To study the dependence of the rotation angle α on the inelasticity, we repeat the computation shown in Sect. 3.2 (same elastic parameters) for inelastic collisions where $A \neq 0$. Figure 6 shows the rotation of the unit vector $\hat{e}_r$ during inelastic collisions over the eccentricity d/l (see Fig. 2) for various dissipative constants A.

In Fig. 7 we additionally fix $d/l = 0.5$ to plot α over the dissipative constant A. To provide a more vivid quantity for the inelasticity of the collision, we give α also as a function of the coefficient of restitution ε corresponding to a central collision at the chosen impact velocity $v_n = \sqrt{3}/2 \cdot 20$ m/s $\approx$ 17.3 m/s [19].

Disregarding for a moment the centrifugal force, the dependence of the moment of inertia on $l(t)$ and the fact that the final deformation $l(\tau)$ depends on A [10], the decreasing function $\alpha(A)$ or $\alpha(\varepsilon)$ may be understood essentially from the fact that the duration of the contact is a decreasing function of inelasticity, $d\tau(A)/dA < 0$. This somewhat unexpected behaviour arises from the fact that a collision terminates when the normal force vanishes (see Eq. 10). That is, the normal force between two inelastically colliding spheres vanishes before the spheres completely relax. Equation (10) then leads to τ being a decreasing function of inelasticity. A rigorous mathematical proof of this relation can be found in [9,10]. Thus, the smaller the coefficient of restitution the shorter lasts the contact and the smaller is the rotation angle during contact. This explanation is certainly oversimplified and serves only as a motivation to understand qualitatively the behavior of $\alpha(A)$.

As shown qualitatively in Fig. 6 and quantitatively in Fig. 7, for all eccentricities the rotation angle adopts its maximum for $A = 0$, corresponding to elastic collisions, $\varepsilon = 1$.

5 Conclusion

For all real materials the collision of particles implies a rotation of the inter-particle unit vector $\hat{e}_r$ during the time of contact τ by a certain angle α. This rotation is neglected in Kinetic Theory of granular systems as well as in event-driven Molecular Dynamics simulations relying both on the hard-sphere model of granular particles. Therefore, to justify the application of the hard-sphere model, one has to assure that the rotation angle is negligible for the given system parameters. In the present paper, we reduce the problem of oblique *elastic* collisions to two independent parameters, $\tilde{l}$ and c_φ, and compute the rotation angle α as a function of these parameters. The result is *universal*, that is, α is known for *any* combination of material parameters (Young modulus Y, Poisson ratio μ, material density ρ_m) and system parameters (particle radii R, impact eccentricity d/l, and impact velocity v).

For dissipative collisions characterized by the coefficient of restitution, $0 < \varepsilon < 1$, we show that the rotation angle is smaller than for the corresponding elastic case where all parameters are the same, except for $\varepsilon = 1$. Therefore, to assess whether the rotation angle is small enough to justify the hard sphere approximation for a given system of dissipative particles, it is sufficient to consider the corresponding system of *elastic* particles discussed in Sect. 3.

For convenient use of our result we provide a universal lookup table and the corresponding access functions (see Online Resource). The angle of rotation for a given situation can be either obtained using the dimensionless variables, $\alpha(c_\varphi, \tilde{l})$, obtained from Eqs. (16) and (17) together with Eqs. (13) and (14) for the present material and system parameters, or by providing the physical parameters directly.

Concluding we consider our result as a tool to assess whether the Kinetic Theory description of a granular system on the basis of the Boltzmann equation and/or its simulation by means of highly efficient event-driven Molecular Dynamics is justified.

Acknowledgments We thank DFG for funding through the Cluster of Excellence 'Engineering of Advanced Materials'.

References

1. Goldhirsch, I.: Rapid granular flow. Ann. Rev. Fluid Mech. **35**, 267–293 (2003)
2. Brilliantov, N.V., Pöschel, T.: Kinetic Theory of Granular Gases. Oxford University Press, Oxford (2010)
3. Pöschel, T., Brilliantov, N. (eds.): Granular Gas Dynamics. Lecture Notes in Physics. Springer, Berlin (2003)
4. Lubachevsky, B.D.: How to simulate billards and similar systems. J. Comp. Phys. **94**(2), 255–283 (1991)
5. Rapaport, D.C.: The event scheduling problem in molecular dynamic simulation. J. Comput. Phys. **34**, 184–201 (1980)
6. Pöschel, T., Schwager, T.: Computational Granular Dynamics. Springer, Berlin (2005)
7. Bannerman, M.N., Sargant, R., Lue, L.: Dynamo: a $O(N)$ general event-driven simulator. J. Comp. Chem. **32**, 3329–3338 (2011)
8. Becker, V., Schwager, T., Pöschel, T.: Coefficient of tangential restitution for the linear dashpot model. Phys. Rev. E **77**, 011304-1–011304-12 (2008)
9. Schwager, T., Pöschel, T.: Coefficient of restitution and linear dashpot model revisited. Granul. Matter **9**, 465–469 (2007)
10. Schwager, T., Pöschel, T.: Coefficient of restitution for viscoelastic spheres: the effect of delayed recovery. Phys. Rev. E **78**, 051304-1–051304-12 (2008)
11. Müller, P., Pöschel, T.: in preparation
12. Hertz, H.: Über die Berührung fester elastischer Körper. J. Reine Angew. Math **92**, 156–171 (1881)
13. Kruggel-Emden, E., Simek, H., Rickelt, S., Wirtz, S., Scherer, V.: Review and extension of normal force modelsfor the discrete element method. Powder Technol. **171**, 157–173 (2007)
14. Stevens, A.B., Hrenya, C.M.: Comparison of soft-sphere models to measurements of collision properties during normal impacts. Powder Techn. **154**, 99–109 (2005)
15. Schäfer, J., Dippel, S., Wolf, D.E.: Force schemes in simulations of granular materials. J. Phys. I France **6**, 5–20 (1996)
16. Brilliantov, N.V., Spahn, F., Hertzsch, J.M., Pöschel, T.: Model for collisions in granular gases. Phys. Rev. E **53**, 5382–5392 (1996)
17. Kuwabara, G., Kono, K.: Restitution coefficient in a collision between two spheres. Jpn. J. Appl. Phys **26**, 1230–1233 (1987)
18. Morgado, W.A.M., Oppenheim, I.: Energy dissipation for quasi-elastic granular particle collisions. Phys. Rev. E **55**, 1940–1945 (1997)
19. Müller, P., Pöschel, T.: Collision of viscoelastic spheres: compact expressions for the coefficient of restitution. Phys. Rev. E **84**, 021302-1–021302-4 (2011)